

Cardiac C-Arm CT: Image-based Gating

C. Rohkohl¹, M. Prümmer¹, R. Fahrig², G. Lauritsch³, J. Hornegger¹

¹ Institute of Pattern Recognition, FA University Erlangen-Nuremberg.

c.rohkohl@oneder.de, {pruemmer, hornegger}@informatik.uni-erlangen.de

² Department of Radiology, Stanford University. fahrig@stanford.edu

³ Siemens AG, Healthcare Sector, Forchheim, Germany. guenter.lauritsch@siemens.com

ABSTRACT

Image guidance during cardiac interventional procedures (IP) using cardiac C-arm CT systems is desirable for many procedures. Applying the concept of retrospective electrocardiogram gating (ECG) to the acquisition of multiple, ECG-triggered rotational acquisitions using a C-arm system allows the 3D+t reconstruction of the heart. The process of retrospective gating is a crucial component of 3-D reconstruction. The gold-standard in gating is still ECG based. However, the ECG signal does not directly reflect the mechanical situation of the heart. Therefore an alternative gating method, based on the acquired projection data is required. Our goal is to provide an image-based gating (IBG) method without ECG such that already acquired projection data from a multi-sweep acquisition can still be used for reconstruction. We formulate the gating problem as a shortest-path optimization problem. All acquired projection images build a directed graph and the path costs are defined by projection image similarities that are based on image metrics to measure the heart phase similarity. The optimization is additionally regularized to prefer solutions where the path segment of consecutive selected projections acquired along a particular forward or backward C-arm sweep is short. This regularization depends on an estimated average heart rate that is also estimated using an image-based method. First promising results using in-vivo data are presented and compared to standard ECG gating. We conclude that the presented IBG method provides a reliable gating.

Keywords: Cardiac C-arm CT, Retrospective Gating, Electrocardiogram-Based Gating, Image-Based Gating

1. INTRODUCTION

Many interventional cardiac procedures are typically interactively assisted by real-time fluoroscopic 2-D images from C-arm based X-ray angiography systems. Cardiac C-arm CT, which is an extension of 3-D rotational angiography,¹ combines 3-D imaging and real-time fluoroscopy in a single system. It can be used to reconstruct high quality 3-D volumes of several cardiac phases. One short-scan (sweep) lasts between 3 to 5 seconds and acquires between 130 to 250 images. The number of cardiac cycles the subject undergoes during a single sweep can range from 2 to over 10. The same anatomical state of the heart in each projection image is a prerequisite for a good reconstruction. Generally, this cannot be guaranteed using only a single sweep short-scan acquisition. In literature^{2,3} this issue is approximately resolved by performing an electrocardiogram (ECG) synchronized multi-sweep scan during venous contrast injection and an ECG-based retrospectively gated reconstruction. More specifically, the C-arm performs K consecutive forward-backward (fw-bw) sweeps, capturing in each sweep exactly N projection images at the C-arm angulations 1 to N (fw) or N to 1 (bw). A gating is comprised by selecting one projection image from the acquired dataset for each angulation that is closest to a reference cardiac phase according to the heart-signal information derived from the ECG.

The electrocardiogram measures the electrical activity during the cardiac cycle. Characteristic wave-forms found in the ECG, mostly the R-peak, are used to derive an electrical cardiac phase. The electrical cardiac phase does not determine the physiological cardiac phase but there exist weak links for example at the R-peak. This allows at normal heart rates for an correlation of the electrical and the physiological cardiac phase. In clinical cases often arrhythmias and highly varying heart rates can be observed which in some cases can pose a problem to the ECG-based gating and may lead to results that could be improved by using image-based gating methods. The use of the acquired projection data via an image-based gating can provide an alternative, as the true physiological heart phase is encoded in the image data. In addition an image-based method can detect undesired patient motion and breathing which is not detectable in the ECG. In seldom cases the ECG recording can be corrupted or missing due to technical reasons which could be handled by an image-based method, too.

In cardiac CT a novel image-based gating method called *Kymogram*⁴ has already been introduced. This method performs gating based on the computed center of gravity of the heart and is therefore sensitive to truncated projection data. In cardiac C-arm CT the projection data is truncated transaxially and therefore new methods are required that are not sensitive to this problem. Blondel *et al.*⁵ determine a cardiac phase from a C-arm image sequence of the coronary artery tree. It is based on the observation that along the cardiac cycle the motion of the coronary tree is characterized by a global bottom-to-top motion. The detector-rows are summed up for each projection image. By minimizing the difference of these horizontal line integrals for two consecutively acquired projection images, the vertical motion component is estimated. For the complete C-arm sweep this results in a curve of the vertical motion versus projection angle which is used to extract cardiac phase information.

In our approach the image-based gating problem is formulated as a shortest-path optimization problem. All acquired projection images build a directed graph and the path costs are defined by projection image similarities that are based on image metrics. To provide an efficient and applicable method we used image metrics that are fast to compute. The optimization is additionally regularized to prefer solutions where consecutive selected projections acquired along a particular C-arm sweep are short. Long consecutive paths along one fw or bw sweep will by definition contain many different heart phases and lead therefore to motion blurring. This regularization depends on an image-based mean heart rate estimation.

This paper is organized as follows: We first introduce a graph-based gating algorithm and additionally present a method to estimate the average heart rate based on the projection images. The computed average heart rate is used as additional regularization of the shortest-path optimization problem. Second, the robustness of the methods is confirmed using in vivo data.

2. METHODS

2.1 Problem Setting

The C-arm acquisition protocol that is used throughout this work takes on the following form:² The C-arm performs K consecutive sweeps, capturing in each sweep exactly N projection images at the same viewing positions. The subject is supposed to breathhold and not to move during the multi-sweep acquisition. Thus, the motion problem is theoretically restricted to cardiac motion.

The projection data $\mathcal{P} = \{p_i^k : i \in \mathbb{N}_N, k \in \mathbb{N}_K\}$, $\mathbb{N}_n = \{1, \dots, n\}$ acquired during a C-arm scan, is the set of all projection images p_i^k acquired at the i -th viewing position during the k -th sweep. For convenience we also refer to the projection images in index notation, i.e. $p_i^k = p_{id(i,k)}$ with $id(i,k) = (j-1)N + i$. This results also into $\mathcal{P} = \{p_l : l \in \mathbb{N}_{N \cdot K}\}$.

Generally, a gating is characterized by a selection of the projection images. More specifically, in this paper the gating selects exactly one projection image for each viewing position, such that each gating provides a complete dataset for a short-scan reconstruction. A projection gating \mathcal{G} in cardiac C-arm CT can be characterized by a N -tuple,

$$\mathcal{G} = (g_1, g_2, \dots, g_N) \quad \text{with} \quad g_i \in \mathbb{N}_K, i \in \mathbb{N}_N$$

with the following interpretation: the element g_i is the number of sweep acquiring the projection image $p_i^{g_i}$ selected in the gating of the i -th viewing position.

2.2 Electrocardiogram-Based Gating

According to Lauritsch *et al.*,^{2,3} after the identification of individual heart beats by R-peak detection in the ECG, the cardiac phase is characterized by the relative distance from the last R-peak. The cardiac phase of the projection p_i is denoted by $\tau(p_i) \in [0, 1]$. An ECG-based gating \mathcal{G}_{τ_r} for the reference cardiac phase τ_r is then given by selecting for each angulation the projection image being closest to the reference phase in a cyclic manner, i.e.

$$\mathcal{G}_{\tau_r} = (g_1, g_2, \dots, g_N) \quad \text{with} \quad g_i = \arg \min_{k \in \mathbb{N}_K} \left\{ \min_{c \in \{0,1,-1\}} |\tau(p_i^k) - \tau_r + c| \right\}. \quad (1)$$

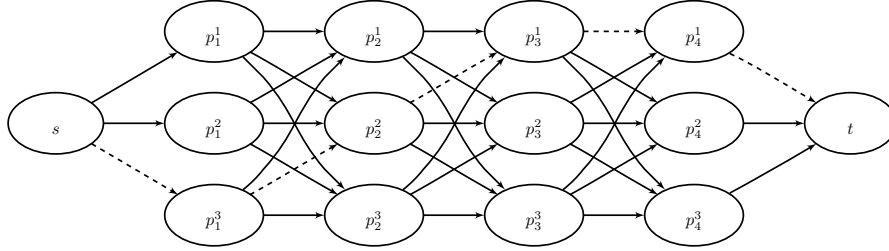


Figure 1. An example projection graph for a C-arm scan with the parameters $N = 4$ and $K = 3$. The graph weights are left out for clarity. The projections along the dashed path are one possible gating. The source is denoted by s and the sink as t , respectively.

2.3 Image-Based Gating Algorithm

2.3.1 Algorithm Description

The foundation of our formulation of image-based gating is the following intuitive observation: Consider the projection data acquired at the C-arm angulations 1 to N . For projections of adjacent angulations the following verbal equation holds:

$$\text{Change of image content} = \underbrace{\text{Sinogram motion}}_{\text{const. for all sweeps}} + \underbrace{\text{Cardiac motion}}_{\text{varies between sweeps}}. \quad (2)$$

The change of image content in neighboring C-arm angulations is composed by the image change due to detector rotation and a change of the cardiac phase. Between adjacent views, the contribution of sinogram motion can be assumed constant and thus to be independent from the C-arm sweeps 1 to K . Contrary, the cardiac phase depends on the particular sweep, as in each sweep the subject was probably in a different cardiac phase. Therefore, one can conclude that the similarity between subsequent C-arm angulations should be minimal for images showing the same physiological cardiac phase. Figure 2 illustrates this situation using difference images from neighboring C-arm angulations. It can be seen that neighboring images with a more similar motion state show less differences than images from a completely different motion state.

This leads to our formulation of the image-based gating algorithm: Find a gating that minimizes the sum of image-based distances d between adjacent projection views, i.e.

$$\mathcal{G}_{\text{IB}} = \arg \min_{(g_1, \dots, g_N)} \sum_{n=1}^{N-1} d(p_n^{g_n}, p_{n+1}^{g_{n+1}}). \quad (3)$$

This formulation can also be interpreted in terms of minimizing the sum of first gradients of the cardiac motion, which is close to zero given the same cardiac phase. This goal can be easily achieved by mapping the minimization task to a weighted directed graph which we call *projection graph* $G = (V, E)$ in the following way: The set of nodes is comprised of two terminals s and t and the projection images, i.e. $V = \{p_1, \dots, p_{NK}, s, t\}$. The set of edges E is constructed by adding an edge from the source s , to the images of the first projection view. An edge is then added for each image from the k -th projection view to all the images from the $k+1$ -th view, the images of the last projection view are connected to the sink t . The directed edges are weighted by an image metric d for any two projection images and by a constant of $c = 1$, if any of the nodes is not a projection image, i.e. a terminal. Figure 1 illustrates the resulting projection graph for a very small artificial scan. Any path connecting the two terminals s and t is a possible gating. The shortest path among them minimizes the sum of distances between adjacent projection views. Efficient algorithms for the shortest path problem in a cycle-free directed graph with non-negative edge-weights are well-known. In this work we utilized Dijkstra's algorithm.⁶ Algorithm 2.1 gives the pseudo-code of a modification including a simple subpath constraint as discussed in Sect. 2.3.4.

For optimal performance of the projection graph approach some prior knowledge is additionally considered. First, the angle increment of successive angulations should be sufficiently small, otherwise the sinogram motion

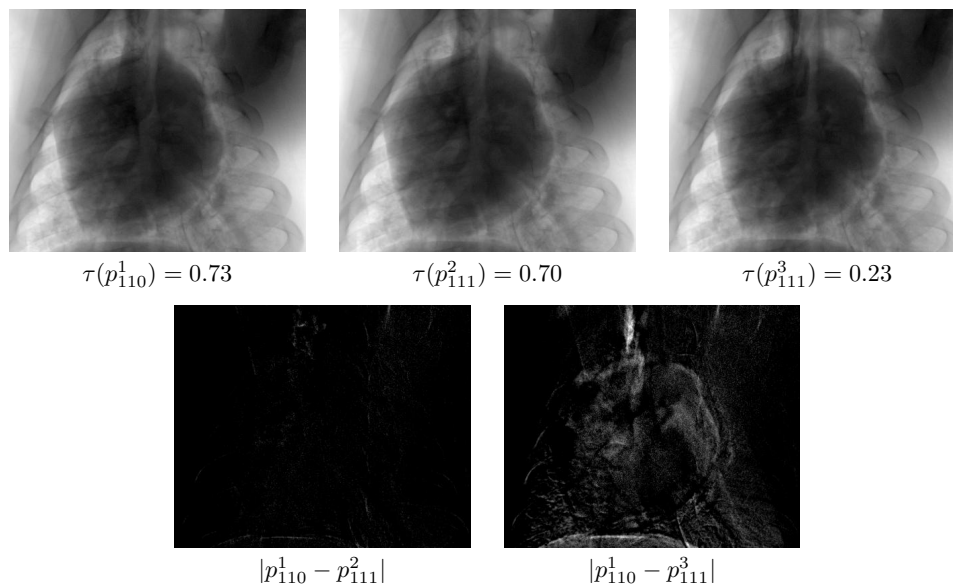


Figure 2. Difference images of neighboring viewing positions from a C-arm scan with the parameters $N = 191$ and $K = 6$. First row: Projection images from the viewing position 110 (first image) and viewing position 111 from different sweeps and with different heart-phases measured from the ECG. Second row: Difference images of projection images from the neighboring viewing positions in the first row. Bright image values indicate a high difference.

dominates and the cardiac phase change becomes negligible. Second, data inconsistencies between the consecutive K C-arm sweeps can additionally distort the before-mentioned relationship and dominate the change in image content. Some factors to consider are noise, the dynamic of contrast agent and non-cardiac motion. This is addressed via projection preprocessing (Sect. 2.3.2) and by the introduction of gating constraints (Sect. 2.3.4).

2.3.2 Image Preprocessing

In accordance to Sect. 2.3.1 the projection data needs to be preprocessed. We decided for the following preprocessing chain (PC) for a projection image p :

1. **[PREP]** Perform the preprocessing of the 3-D reconstruction algorithm and select the images that directly contribute to the calculation of the 3-D volume. This preprocessing generally includes, but is not limited to, correction algorithms for scatter, beam hardening, truncation and ring artifacts. In our implementation the preprocessing of the reconstruction algorithm presented in¹ is used.
2. **[SCALE]** Downscale the images to speed up the calculation.
3. **[FILTER]** Due to the detector rotation between neighboring angulations joint structures such as edges do not exactly overlap. To compensate for this difference a low-pass filter e.g. a Gauß filter kernel, is applied.
4. **[GRAD]** (optional) Calculate the magnitude of the image gradient. The image gradient provides structural information of the heart geometry.
5. **[ROI]** The sinogram motion is spread over the complete projection image. To minimize its contribution the projection images are cropped to a user-supplied region of interest (ROI) of p that contains the complete heart in all projection images and heart phases.

Figure 3 illustrates the preprocessing steps applied to the projection data. In the following we denote the preprocessing chain without gradient computation PC and with gradient computation PC+[GRAD].

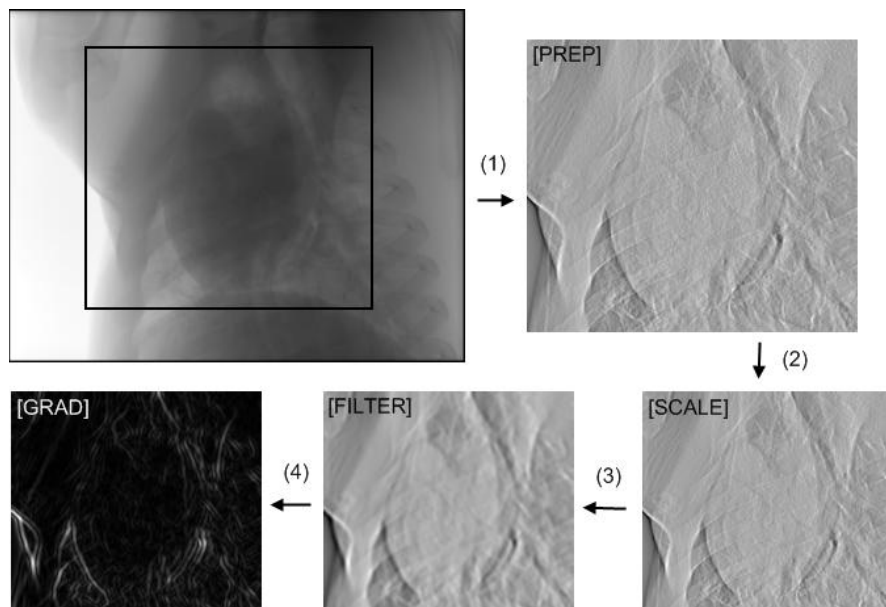


Figure 3. Preprocessing chain applied to the projection data. The arrows indicate the processing direction starting from the original projection image. The step [ROI] is indicated by the black square in the original image and is blended out in the following images.

2.3.3 Distance Metrics

In general any grayscale image metric can be used as the distance measure d in the image-based gating algorithm. In our experiments three different distance measures have been tested: the Euclidean distance, the correlation coefficient and an SVD-based measure.⁷ We provide results for the Euclidean distance only, as it provided stable results at low computational costs.

2.3.4 Introducing Gating Constraints

To further improve the gating result we introduce a regularization of the length of consecutively selected projections from the same C-arm sweep. This length depends on the mean heart rate that is also estimated based on the provided image information. We therefore introduce the possibility to perform a simple constrained shortest path search using Dijkstra's⁶ algorithm. At any step of Dijkstra's path search, to each possible subpath under consideration an additional validity value v is added to the actual path costs. Algorithm 2.1 gives the pseudo code for the modified path search. The only change to the standard algorithm is in lines 17-18, where the validity value v is returned by the function *validity*. The validity value is zero for valid gatings and infinity for non-valid gatings. A path is valid if within a time-frame of w , not more than m projection images from a particular sweep have been selected. This allows to select only reasonable solutions regarding the characteristics of the cardiac cycle. From physiology⁸ it is known, that specific cardiac phases are fixed to a certain amount of time, which can be enforced with the introduced validity value.

By experience, the mean heart rate \hat{H} and the mean time ΔT between two subsequently acquired projection images (determined by the acquisition protocol), provide a good intuition on how to parametrize the validity constraints. The mean heart rate allows for the determination of an upper bound for the diastolic (or systolic) duration. We have found the following heuristic suitable to parametrize a gating

$$w = 0.65 \cdot \frac{1}{\hat{H}}, \quad m = 0.65 \cdot \frac{w}{\Delta T}.$$

It ensures that no more than 65% of the projections during a fraction of 65% of the cardiac cycle time are selected from a particular sweep. The mean heart rate is patient specific and needs to be inferred from the image data,

for a purely image-based algorithm. A method for the image-based mean heart rate estimation is presented in Sect. 2.4.

Algorithm 2.1 Modified version of Dijkstra's algorithm for finding the shortest path in the projection graph $G = (V, E)$. The function *getpath* creates the shortest path by iterating through the predecessor map P . The function *validity* returns the validity value for a subpath. For more details on the modifications refer to Sect. 2.3.4.

```

1:  $P \leftarrow \emptyset$  // Predecessors of any node on shortest path to that node
2:  $D_s(s) \leftarrow 0$  // Costs for reaching an node from the source
3:  $Q \leftarrow V$  // Set of nodes to be examined
4: for all  $u \in V$  such that  $u \neq s$  do
5:    $D_s(u) \leftarrow +\infty$ 
6: end for
7: while  $Q \neq \emptyset$  do
8:   find  $u \in Q$  such that  $D_s(u) = \min_{u' \in Q} (D_s(u'))$ 
9:    $Q \leftarrow Q \setminus u$ 
10:  for all Neighbors  $v \in Q$  of  $u$  do
11:    if  $u = s$  or  $v = t$  then
12:       $a \leftarrow 1$ 
13:    else
14:       $a \leftarrow d(u, v)$ 
15:    end if
16:     $subpath = getpath(P, u) \cup v$ 
17:    if  $D_s(u) + a + validity(subpath) < D_s(v)$  then
18:       $D_s(v) \leftarrow D_s(u) + a + validity(subpath)$ 
19:       $P(v) = u$ 
20:    end if
21:  end for
22: end while
23: return  $getpath(P, t)$ 

```

2.4 Image-Based Mean Heart Rate Estimation

During a forward sweep, the C-arm rotates from angulation 1 to N and pauses for a certain amount of time. Then the backward sweep starts and collects again images, now in reverse order at the angulations N to 1. The upper graph in Fig. 4 shows the ECG measured cardiac phase versus the acquisition time. At constant heart rates typically two intersections per cardiac cycle can be observed. Figure 4 (lower image, dotted) shows the normalized distance between the pairs of projection images at the same angulations. The distance for two projections p_1, p_2 is given by $\min_{c \in \{0,1,-1\}} |\tau(p_1) - \tau(p_2) + c|$. The solid curve in Fig. 4 (lower image) shows the normalized image-based distance measure d for the same pairs of projection images. Clearly the set of time instants where the cardiac phase of a fw-bw run combination is equal, corresponds to a minima of the image-based distance function. The core idea of our image-based mean heart rate estimation algorithm is to emulate an artificial heart signal which shows the same set of intersections. The algorithm works as follows:

Let L in the following denote the number of all fw-bw sweep combinations. In the first phase of our algorithm for each of the L fw-bw sweep combinations the image-based distance curve is determined. For each of the curves the set of the local minima R_i are detected. The set of all combinations is $\mathbf{R} = \{R_1, \dots, R_L\}$.

In the second phase of our algorithm we create an artificial heart signal with an assumed constant heart rate h . Thus, for each fw-bw sweep combination a plot similar to the top of Fig. 4 can be created with that artificial heart signal. Next, the minima $\mathbf{A}_h = \{A_1^h, \dots, A_L^h\}$ for each of the fw-bw sweep combinations are calculated by finding the heart phase intersections in the artificial signal.

For a quality measure used to estimate the correspondence between \mathbf{R} and any \mathbf{A}_h a triangular function $\lambda_M(x)$ is introduced which is created for any set of minima M of \mathbf{R} or \mathbf{A}_h . It takes on the value 1 if x is

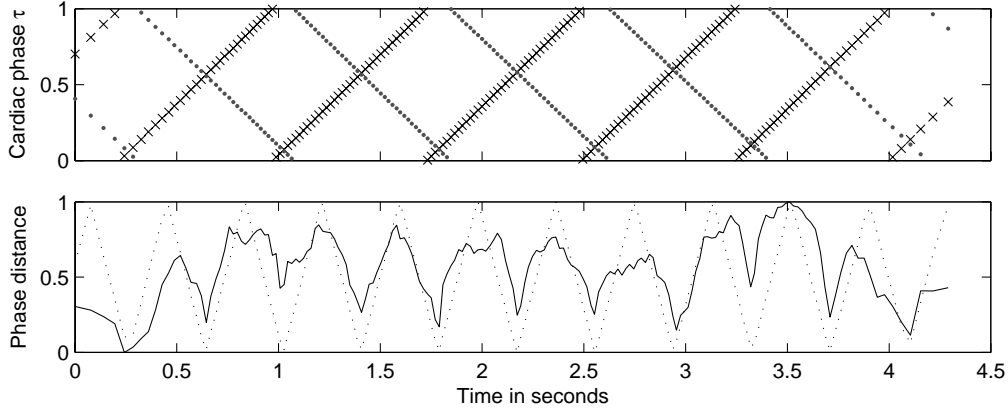


Figure 4. Illustration of average heart rate estimation. The top image shows the ECG measured relative heart phases from a forward sweep (\bullet) and a backward sweep ($+$). The bottom image shows the phase distance between the ECG-based heart phases of each projection pair from the fw-bw sweep (dotted) and the image-based distance using the distance measure d (Euclidean distance) of the same image pairs. All values are normalized to lie within $[0, 1]$.

a minimum, 0 if x lies in the middle of two consecutive minima and a linearly interpolated value in-between. Visually speaking this function is a triangle of height one centered around each minima. Using λ_M we can define the following objective function

$$\epsilon(h) = \sum_{i=1}^L \int (\lambda_{R_i}(x) - \lambda_{A_i^h}(x))^2 dx, \quad (4)$$

which measures the squared difference of the reference and artificial minima triangular functions for all fw-bw sweep combinations. The minimization of ϵ is done by discretizing the search space $[h_{\min}, h_{\max}]$ and performing an exhaustive search. The optimal heart rate h is interpreted as the mean heart rate. In order to stabilize the estimated mean heart rate, a certain fraction of the best optimized heart rates are averaged.

3. PRECLINICAL STUDIES IN AN ANIMAL MODEL

3.1 Methods and Materials

The data used in this study was acquired using an in vivo porcine model. Six sweeps were acquired in an alternating forward/backward order, (191 projections per 4s sweep, matrix size 620×480 , 60 frames/s, angular increment 1° , $\Delta T = 0.02s$) resulting in a total of 1146 projection images. Nine different datasets were acquired. During the preprocessing chain a scaling to 60% of the image size ([SCALE]) and a Gauß filter kernel of size 5×5 with a standard deviation of 2 ([FILTER]) have been applied.

We performed reconstructions using an end-diastolic electrocardiogram-based nearest neighbor gating (M1) at $\tau_r = 0.75$ and four different configurations M2-M5 of the introduced image-based gating method. In total 45 gated and 9 non-gated reconstructions have been examined. Table 1 gives an overview of the gating methods M1-M5.

In order to quantify the effects of the gatings, four experts were asked in an image quality survey to rate the quality between the non-gated reconstruction using the projection images of the first C-arm sweep and

1. a gated reconstruction using image-based gating and
2. ECG-based gating as reference.

We presented two anonymized MPR-slices with common visualization configurations (slice thickness, slice orientation, grayscale window) and instructed the experts to grade image 2 in comparison to image 1 with a whole number between -3 and 3, with -3 being much worse and 3 being much better. The order of the displayed images

was completely random. The user rating was converted, such that always the gated version could be regarded as image 2.

Table 1. Overview of the gating methods M1-M5 used in the evaluation.

Method	Gating Type	Constrained	Preprocessing
M1	$\mathcal{G}_{\tau_r=0.75}$ (ECG)	–	–
M2	\mathcal{G}_{IB}	no	PC
M3	\mathcal{G}_{IB}	no	PC+[GRAD]
M4	\mathcal{G}_{IB}	yes	PC
M5	\mathcal{G}_{IB}	yes	PC+[GRAD]

3.2 Results: Image-Based Gating

Exemplary reconstruction results of the subjects 1,2,5,7 are depicted in Figs. 6-9. The upper-left image shows the reconstruction result of the non-gated reconstruction. The second image (from left to right) shows the gated reconstruction using the ECG information (M1). The other images show the gated reconstruction results using the four different configurations (M2-M5) of our image-based gating algorithm.

3.2.1 Gating Selection

In all reconstruction results, except one (Subject 1, M3, Fig. 6), a diastolic phase has been determined by the image-based algorithms. This is expectable due to the well-known fact of the diastolic phase being motion-poor.

3.2.2 Image Quality Survey

Figure 5 shows the average score for each method and each subject. Table 2 lists the scores for each method averaged over all datasets.

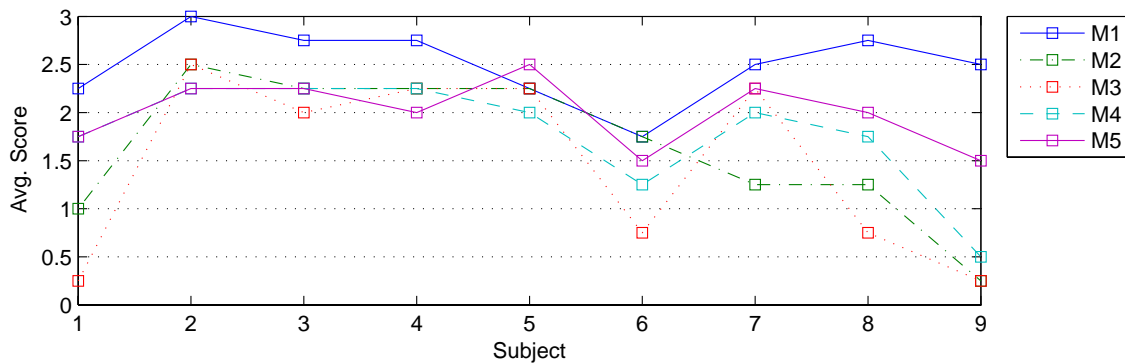


Figure 5. Graphical overview of the average method score for each subject.

Table 2. Overall evaluation results for the methods M1-M5 for all subjects.

	M1	M2	M3	M4	M5
Total Avg. Score	2.50	1.64	1.47	1.78	2.00

Method M1 The current gold standard for cardiac 3-D reconstruction is the electrocardiogram-based gating which was also confirmed by our evaluation study. It is most reliable and with an average score of 2.5 it is superior to the best image-based method with a score of 2.0. For the subjects 5 and 6 an equal or better scoring could be reached by image-based methods.

Table 3. Results of the image-based average heart rate estimation versus the measured electrocardiogram mean heart rates. All values are given in beats per minute (bpm).

Subject	1	2	3	4	5	6	7	8	9
ECG	94.20	78.87	75.87	86.76	77.15	76.71	79.40	82.47	83.95
IB	94.50	79.00	73.75	86.90	78.00	76.30	80.90	82.25	84.50
Error	0.23	0.13	2.12	0.14	0.85	0.41	1.45	0.22	0.55
Avg. Error	0.69 bpm								

Methods M2,M3 The unconstrained image-based methods M2,M3 are generally less reliable compared with their constrained counterparts M4,M5. This is most likely due to the selection of too many consecutive projections of the same C-arm sweep and a mixture of different cardiac phases.

Methods M4,M5 The constrained methods M4,M5 outperformed their non-constrained versions. Especially the boost of M3 to M5 with an average score of 1.47 to 2.0 shows that the preprocessing of the image data with the combination of gating constraints improve the gating quality.

3.3 Results: Image-Based Mean Heart Rate Estimation

The results for the image-based average heart rate estimation are depicted in Tab. 3. The presented method provides a reasonable estimation of the average heart rate during image acquisition with an average error of 0.69 bpm for the 9 tested animal datasets using a measured ECG signal as gold-standard for evaluation. It hence allows for the integration of a proper constraint into the image-based gating algorithm.

4. DISCUSSION

The direct visual comparison of the ECG-based and image-based gated reconstructions reveals that for a wide range of the results the image-based method can compete with the ECG-based gating. For examples see Figs. 6-9. For the cases under consideration the electrical cardiac phase correlated well with the physiological cardiac phase and hence good ECG-gated reconstructions could be achieved. Further investigations are required specifically in cases with deviations during the cardiac cycle which are weakly correlated to the electrical heart phase. Candidates are patients with arrhythmias or highly varying heart rates, or cases that are corrupted due to factors that cannot be measured by the ECG, e.g. non-cardiac motions as breathing or patient displacements.

5. SUMMARY AND CONCLUSION

In this work a novel image-based gating algorithm has been presented as an alternative to electrocardiogram-based gating in cardiac C-arm CT. The image-based algorithm is based on the projection data only. Different preprocessing steps are applied. Four different configurations of the image-based algorithm including variations of the preprocessing and a validity constraint for gatings, have been evaluated. An image-quality survey on the reconstructions of an animal study with nine different subjects was carried out. As reference an end-diastolic ECG-gated reconstruction was performed. In all but one reconstruction result, a diastolic phase has been determined by the image-based algorithms which confirms that image-based gating naturally selects cardiac phases from a period of no motion. According to our evaluation the best image-based method (M5) used structure information (gradient) in the calculation of projection image similarities and a path constraint based on the mean heart rate. Two reconstructions results of the image-based gating (subjects 5,6) received an equal or better score than the ECG-based method. However, the reference ECG-based gating still gained slightly better scores in many cases. The reason might be seen in the selection of cases with stable and regular heart signals. Evaluating more challenging cases with irregular, arrhythmic heart signals is work in progress.

For the regularization of our image-based gating an image-based mean heart rate estimation procedure has been introduced. For the nine examined datasets an average deviation of 0.69 bpm from the mean heart rates derived from the ECG was observed.

We draw the conclusion that the image-based algorithm presented herein can provide a high quality gated 3-D reconstruction of the heart.

ACKNOWLEDGMENTS

We thank Wendy Baumgardner and Diane Howard for technical assistance at Stanford University. This research is supported by NIH R01 EB003524, Siemens AG, and the Lucas Foundation.

DISCLAIMER

The concepts and information presented in this paper are based on research and are not commercially available.

REFERENCES

1. M. Zellerhoff, B. Scholz, E.-P. Ruehrnschopf, and T. Brunner, "Low contrast 3d reconstruction from c-arm data," in *Medical Imaging 2005: Physics of Medical Imaging. Proceedings of the SPIE.*, M. J. Flynn, ed., **5745**, pp. 646–655, Apr. 2005.
2. G. Lauritsch, J. Boese, L. Wigstrm, H. Kemeth, and R. Fahrig, "Towards cardiac c-arm computed tomography," *IEEE Transactions on Medical Imaging* **25**, pp. 922–934, July 2006.
3. G. Lauritsch, J. Boese, L. Wigstroem, M. Prümmer, and R. Fahrig, "Temporal resolution in cardiac c-arm ct in the presence of variable heart rate.," in *9th Int. Meeting on Fully 3D Image Reconstruction in Radiology and Nuclear Medicine*, pp. 358–361, 2007. Linday, Germany.
4. M. Kachelrieß, D. Sennst, W. Maxlmoser, and W. Kalender, "Kymogram detection and kymogram - correlated image reconstruction from subsecond spiral computed tomography scans of the heart," *Medical Physics* **29**(7), pp. 1489–1503, 2002.
5. C. Blondel, G. Malandain, R. Vaillant, and N. Ayache, "Reconstruction of coronary arteries from a single rotational x-ray projection sequence," *IEEE Transactions on Medical Imaging* **25**, pp. 653–663, May 2006.
6. E. W. Dijkstra, "A note on two problems in connexion with graphs," in *Numerische Mathematik*, **1**, pp. 269–271, Mathematisch Centrum, Amsterdam, The Netherlands, 1959.
7. A. Shnayderman, A. Gusev, and A. Eskicioglu, "An svd-based grayscale image quality measure for local and global assessment," *IEEE Transactions on Image Processing* **15**, pp. 422–429, February 2006.
8. R. E. Klabunde, *Cardiovascular Physiology Concepts*, Lippincott Williams & Wilkins, July 2004. <http://www.cvphysiology.com>.

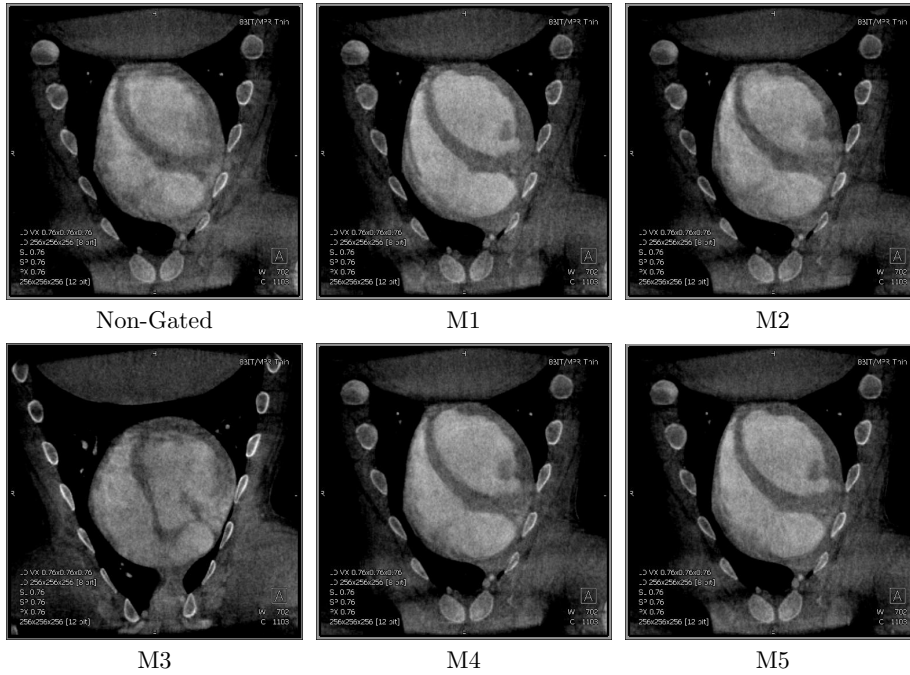


Figure 6. Subject 1: MPR views of the 3-D Reconstruction results. Grayscale window: $w = 702$, $c = 1103$.

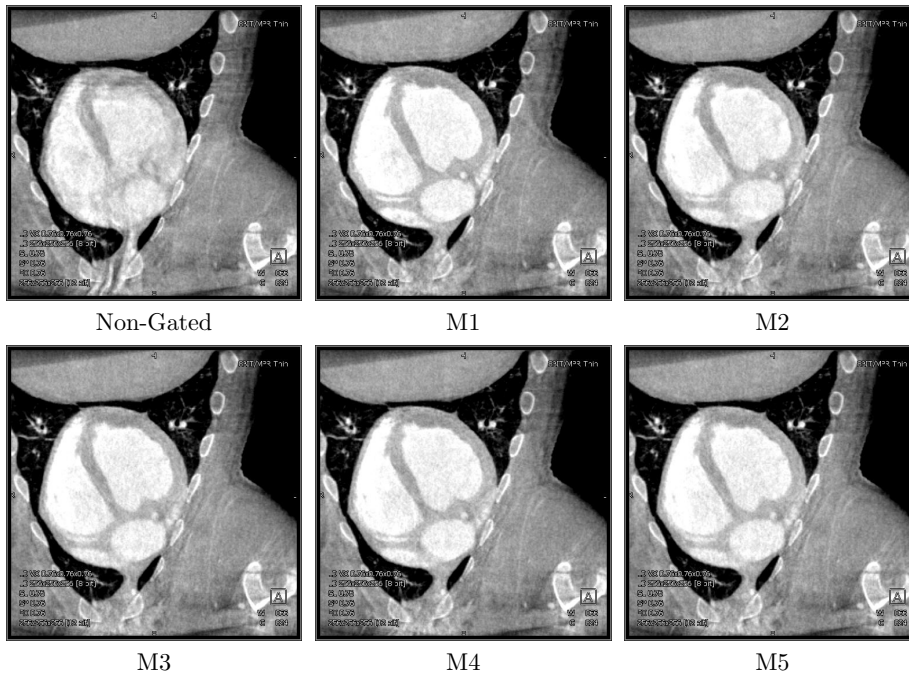


Figure 7. Subject 2: MPR views of the 3-D Reconstruction results. Grayscale window: $w = 866$, $c = 824$.

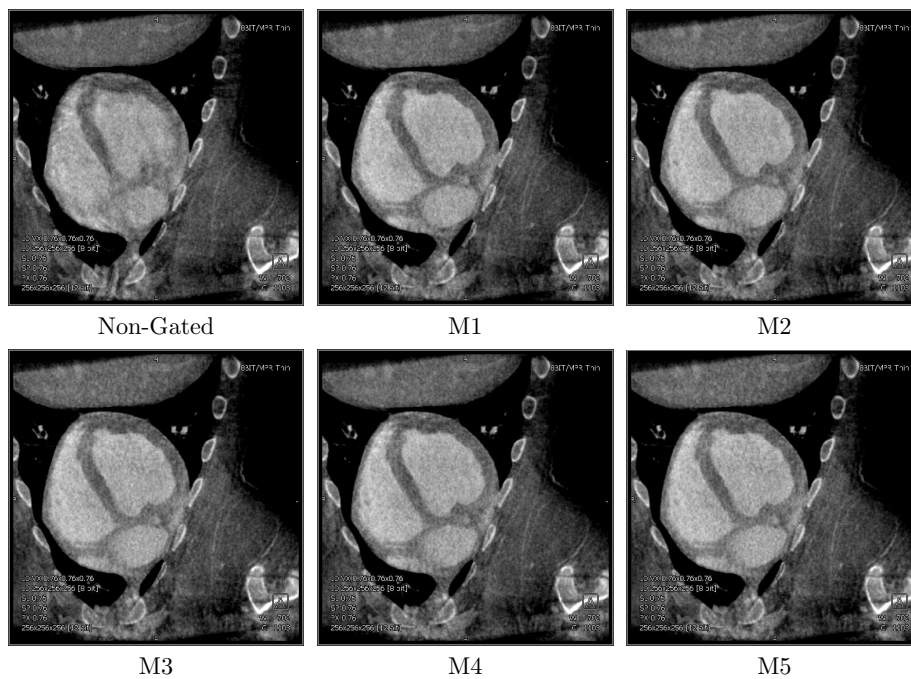


Figure 8. Subject 5: MPR views of the 3-D Reconstruction results. Grayscale window: $w = 702$, $c = 1103$.

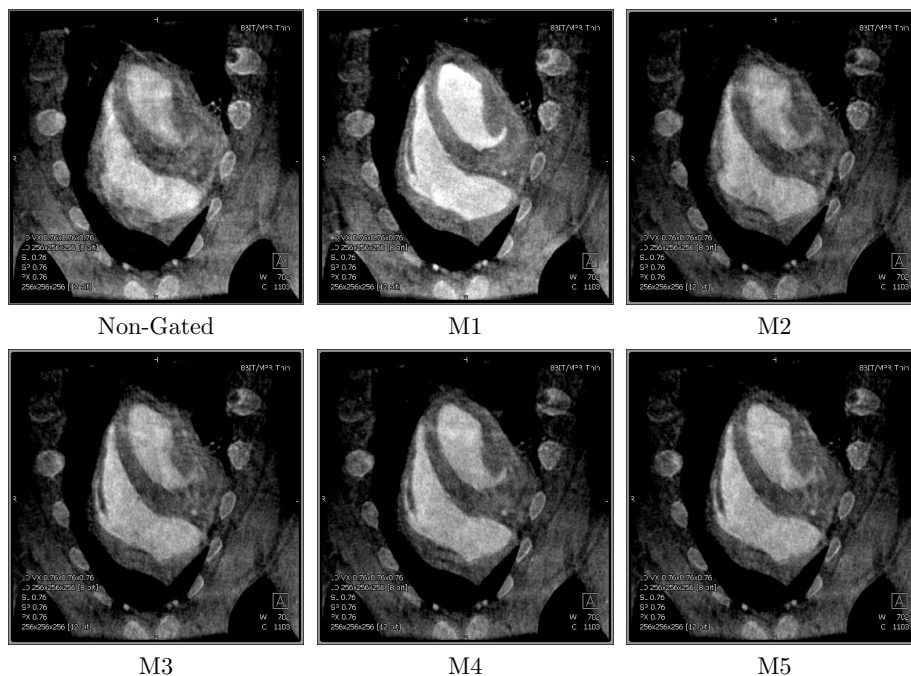


Figure 9. Subject 7: MPR views of the 3-D Reconstruction results. Grayscale window: $w = 702$, $c = 1103$.